Simple Electromagnetic Modeling Procedure: From Near-Field Measurements to Commercial Electromagnetic Simulation Tool

Priscila Fernández López, Christian Arcambal, David Baudry, Serge Verdeyme, *Member, IEEE*, and Bélahcène Mazari, *Member, IEEE*

***Abstract*—As the first part of a study that aims to propose tools to take into account some electromagnetic compatibility aspects, we have developed a model to predict the electric and magnetic fields emitted by a device. This model is based on a set of equivalent sources (electric and magnetic dipoles) obtained from the cartographies of the tangential components of electric and magnetic near fields. One of its features is to be suitable for a commercial electromagnetic simulation tool based on a finite element method. This paper presents the process of modeling and the measurement and calibration procedure to obtain electromagnetic fields necessary for the model; the validation and the integration of the model into a commercial electromagnetic simulator are then performed on a Wilkinson power divider.**

***Index Terms*—Circuit modeling, dipole arrays, electromagnetic compatibility (EMC), electromagnetic measurements, simulation software.**

I. Introduction

TO take into account the electromagnetic compatibility (EMC) in the first steps of the design of an electronic board, we need to study its radiated emissions. Indeed, the radiation of components, tracks, or cables of a board can induce parasitic voltages or currents in the same board or in a neighbor one. Moreover, this radiation has to be also compliant with the limits defined in the standards.

To estimate the fields, some radiated electromagnetic measurements can be performed with a near-field test bench. This characterization tool has several applications on the EMC. In [1], near-field measurements are used to locate the regions of high or low fields radiated by a board and to evaluate the shielding efficiency locating faults in a cable. An estimation of the current flowing in a circuit is done in [2]. The far-field prediction is studied in [3] where the magnetic near-field measurements and some information about the geometry of the circuit are used. In [4], the authors calculate an equivalent magnetic current from the electric near-field measurements to estimate the far-field radiation of aperture antennas. Another application is the development of radiation models.

Concerning this application, electronics engineers become more and more interested in component models, particularly due to the increasing computational power and the development of high performance commercial electromagnetic simulation software. Thus, for several years, some radiated electromagnetic models of components have been created. They are usually composed of equivalent sources (electric and/or magnetic dipoles) that radiate the same field as the device under test (DUT). Several techniques have been developed to obtain these sources: a genetic algorithm [5], a comparison of the magnetic field radiated by the DUT to the radiation of a circular loop [6], a metaheuristic method [7], an image processing associated with an optimization algorithm [8], the knowledge of the internal architecture for certain integrated circuits [9], or a super-resolution method based on the equivalence principle [10]. The models allow the prediction of fields, the study of certain configurations, such as the presence of a conductor close to the modeled circuit [11], and the possible couplings with another equipment.

These objectives are also our final goals, and we also want to make the model suitable for certain commercial electromagnetic simulation tools. The model can be easily obtained with a mathematical code, such as Matrix Laboratory (MATLAB) [12], from the analytical expressions of the dipoles' radiation and a least-square inverse method. The predicted fields can be used as the field data input for the Taylor model to calculate the induced voltages in a transmission line disturbed by the field [13]. However, the model can be also used in commercial electromagnetic software, such as High-Frequency Structure Simulator (HFSS) and Computer Simulation Technology (CST) Microwave Studio.

In the first part of our research, we focus on the modeling of simple structures to validate our procedure. The model is not necessarily a single unique solution; indeed, it only has to be able to predict fields with a certain accuracy defined by the user. In a previous work, we developed a methodology of modeling which predicts the magnetic field radiated by

Manuscript received July 31, 2009; revised March 1, 2010; accepted March 2, 2010. Date of current version November 10, 2010. The Associate Editor coordinating the review process for this paper was Dr. Sergey Kharkovsky.

P. Fernández López is with the Embedded Electronic Systems Research Institute (IRSEEM), 76801 Saint Etienne du Rouvray, France and also with the University of Rouen, 76821 Mont Saint Aignan, France (e-mail: p.fernandez-lopez@esigelec.fr).

C. Arcambal is with Commisariat à l'énergie atomique et aux énergies alternatives, Centre de Saclay, 91191 Gif-sur-Yvette, France (e-mail: christian.arcambal@cea.fr).

D. Baudry and B. Mazari are with the Embedded Electronic Systems Research Institute (IRSEEM), 76801 Saint Etienne du Rouvray, France (e-mail: baudry@esigelec.fr; mazari@esigelec.fr).

S. Verdeyme is with XLIM Laboratory, University of Limoges, 87060 Limoges, France (e-mail: serge.verdeyme@xlim.fr).

Digital Object Identifier 10.1109/TIM.2010.2063070

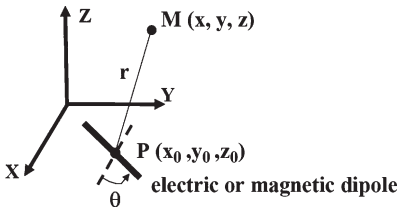

Fig. 1. Electric or magnetic dipole in the xy plane.

an electronic device (active or passive) [14]. We have then completed it to predict both the electric and magnetic fields using a single model. The aim is to propose a model that is easy to be built and is used by engineers without information about the internal architecture of the device. Thus, our research is particularly focused on the compatibility of our model with existing electromagnetic simulation software.

In this paper, we present the completed model based on a set of equivalent sources that radiates the same near electric and magnetic fields as the device to be modeled. To obtain it, the near-field cartographies of the electric ($\vec{E}$) and magnetic ($\vec{H}$) fields emitted by the component are needed. The measurement procedure is discussed in Section III, focusing on the probes used and their calibration. A Wilkinson power divider is then characterized in Section IV to validate the process of modeling, and afterward, its model is inserted into a commercial electromagnetic simulation tool based on the finite element method. Some aspects of our modeling procedure, such as the limitations, are discussed in Section V.

II. Presentation of the Model

Our modeling procedure has been tested on some electronic components and boards (active or passive) working between 40 and 1 GHz without information about their internal architecture or topology, i.e., the component can be considered as a black box. In the first step of our study, we are interested in the electromagnetic field above the component.

A. Principle of the Model

The model is based on a set of elementary sources (electric and magnetic dipoles) placed on an xy plane considered as the upper surface of the highest component of the board. Some of the parameters of the dipoles are fixed: the number, their positions, and their lengths. The frequency is also considered as a parameter. Thus, one model is developed for each frequency and corresponds to a specific working of the device. The unknown variables of the model are the orientations θ_e and the currents I_e (magnitude and phase) for the electric dipoles and the orientations θ_m and the currents I_m (magnitude and phase) for the magnetic dipoles (see Fig. 1).

B. Mathematical Analysis

To build the model, we use the expressions of the electric and magnetic fields radiated at a point M by an electric dipole (from magnetic vector potential $\vec{A}$) and by a magnetic dipole (from electric vector potential $\vec{F}$) [14], [15]. Thus, the different components ($p = \{x, y, z\}$) of the electric and magnetic fields emitted by an electric dipole can be expressed as follows:

$$E_{A,p} = f_p(k, x, y, z, x_0, y_0, z_0, l, I_e, \theta_e, \varepsilon) \tag{1}$$

$$H_{A,p} = g_p(k, x, y, z, x_0, y_0, z_0, l, I_e, \theta_e) \tag{2}$$

and the fields emitted by a magnetic dipole are

$$E_{F,p} = -\,g_p(k, x, y, z, x_0, y_0, z_0, l, I_m, \theta_m) \tag{3}$$

$$H_{F,p} = f_p(k, x, y, z, x_0, y_0, z_0, l, I_m, \theta_m, \mu) \tag{4}$$

where f and g are two functions depending on the following variables.

1) (x, y, z) are the coordinates of the point M where the electromagnetic field is evaluated.
2) (x_0, y_0, z_0) are the coordinates of the center of the dipole.
3) l corresponds to its length.
4) k is the wavenumber ($2\pi/\lambda$, where λ is the wavelength).
5) ε and μ are the permittivity and permeability of the medium, respectively.
6) I_e (or I_m) is the electric (or magnetic) current through the electric (or magnetic) dipole in amperes (or volts).
7) θ_e (or θ_m) represents the orientation of the electric (or magnetic) dipole in the xy plane.

Fig. 1 shows an electric or magnetic dipole in the xy plane describing these parameters.

The total $\vec{E}$ and $\vec{H}$ fields are given by the contribution of each elementary dipole (N_e electric dipoles and N_m magnetic dipoles)

$$E_p = \sum_{i=1}^{N_e} E_{A,p,i} + \sum_{j=1}^{N_m} E_{F,p,j} \tag{5}$$

$$H_p = \sum_{i=1}^{N_e} H_{A,p,i} + \sum_{j=1}^{N_m} H_{F,p,j}. \tag{6}$$

To determine the unknown parameters of the model, the cartographies of the near-field tangential components E_x, E_y, H_x, and H_y (amplitude and phase) at a certain height d above the device are required. Then, the problem is represented as a matrix system

$$\begin{pmatrix} [E_x] \\ [E_y] \\ [H_x] \\ [H_y] \end{pmatrix} = \begin{pmatrix} \alpha_{1,1} & \cdots & \alpha_{1,s} \\ \vdots & \ddots & \vdots \\ \alpha_{r,1} & \cdots & \alpha_{r,s} \end{pmatrix} \begin{pmatrix} [I_e \sin(\theta_e)] \\ [I_e \cos(\theta_e)] \\ [I_m \sin(\theta_m)] \\ [I_m \cos(\theta_m)] \end{pmatrix} \tag{7}$$

where the $\alpha_{i,j}$ elements depend on the frequency and the centers and lengths of the dipole, $r/4$ is the number of measurement points at the space of each component of the field (E_x, E_y, H_x, and H_y), and $s/2$ is the total number of equivalent sources.

This type of problem ($b = Ax$) is called an inverse problem, and it can be ill-conditioned, which means that the computed solution x is potentially very sensitive to disturbances from the measured data b. To improve the status of the matrix in terms of

the condition number, the measured fields and their respective rows in the matrix $[\alpha]$ are normalized (noted as n) as follows:

$$\begin{pmatrix}[E_x]\\[E_y]\\[H_x]\\[H_y]\end{pmatrix}_n = [E,H]_n = \begin{pmatrix}\left[\frac{E_x}{\max(|E_x|)}\right]_{\frac{r}{4}\times 1}\\ \left[\frac{E_y}{\max(|E_y|)}\right]_{\frac{r}{4}\times 1}\\ \left[\frac{H_x}{\max(|H_x|)}\right]_{\frac{r}{4}\times 1}\\ \left[\frac{H_y}{\max(|H_y|)}\right]_{\frac{r}{4}\times 1}\end{pmatrix} \tag{8}$$

$$[\alpha]_n = \begin{pmatrix}\begin{bmatrix}\frac{\alpha_{1,1}}{\max(|E_x|)} & \cdots & \frac{\alpha_{1,s}}{\max(|E_x|)}\\ \vdots & \ddots & \vdots\\ \frac{\alpha_{r/4,1}}{\max(|E_x|)} & \cdots & \frac{\alpha_{r/4,s}}{\max(|E_x|)}\end{bmatrix}_{\frac{r}{4}\times s}\\ \begin{bmatrix}\frac{\alpha_{r/4+1,1}}{\max(|E_y|)} & \cdots & \frac{\alpha_{r/4+1,s}}{\max(|E_y|)}\\ \vdots & \ddots & \vdots\\ \frac{\alpha_{r/2,1}}{\max(|E_y|)} & \cdots & \frac{\alpha_{r/2,s}}{\max(|E_y|)}\end{bmatrix}_{\frac{r}{4}\times s}\\ \begin{bmatrix}\frac{\alpha_{r/2+1,1}}{\max(|H_x|)} & \cdots & \frac{\alpha_{r/2+1,s}}{\max(|H_x|)}\\ \vdots & \ddots & \vdots\\ \frac{\alpha_{3r/4,1}}{\max(|H_x|)} & \cdots & \frac{\alpha_{3r/4,s}}{\max(|H_x|)}\end{bmatrix}_{\frac{r}{4}\times s}\\ \begin{bmatrix}\frac{\alpha_{3r/4+1,1}}{\max(|H_y|)} & \cdots & \frac{\alpha_{3r/4+1,s}}{\max(|H_y|)}\\ \vdots & \ddots & \vdots\\ \frac{\alpha_{r,1}}{\max(|H_y|)} & \cdots & \frac{\alpha_{r,s}}{\max(|H_y|)}\end{bmatrix}_{\frac{r}{4}\times s}\end{pmatrix}. \tag{9}$$

The least-square inverse method and a division element by element are used to obtain the orientations θ_e and θ_m

$$[\alpha]_n^{-1}[E,H]_n = \begin{pmatrix}[I_e\sin(\theta_e)]\\ [I_e\cos(\theta_e)]\\ [I_m\sin(\theta_m)]\\ [I_m\cos(\theta_m)]\end{pmatrix} = \begin{pmatrix}[A]\\[B]\\[C]\\[D]\end{pmatrix} \tag{10}$$

$$\theta_e = arctg\left(\frac{[A]}{[B]}\right) \tag{11}$$

$$\theta_m = arctg\left(\frac{[C]}{[D]}\right). \tag{12}$$

After obtaining these parameters, a new matrix $[\beta]$ is defined. Its elements not only depend on the space coordinates but also on θ_e and θ_m

$$\begin{pmatrix}[E_x]\\[E_y]\\[H_x]\\[H_y]\end{pmatrix} = \begin{pmatrix}\beta_{1,1} & \cdots & \beta_{1,s/2}\\ \vdots & \ddots & \vdots\\ \beta_{r,1} & \cdots & \beta_{r,s/2}\end{pmatrix}\begin{pmatrix}[I_e]\\[I_m]\end{pmatrix}. \tag{13}$$

The normalization is also carried out now for the measurement vector and for the matrix $[\beta]$ as in (8) and (9). We then use the least-square inverse method to obtain I_e and I_m.

When all the parameters of the model are determined, it is possible to calculate the electric and magnetic fields at any other height in the near-field region above which the cartographies were obtained (d).

To find the unknown parameters of the model, some optimization methods can be used, but they quickly make the modeling procedure complex and slow due to the increasing number of variables [16]. Therefore, even if the problem solved by a least-square inverse method presents some drawbacks with the condition number, this method is used because of its quickness: obtaining the model only takes a few seconds.

Once the model is built, we can use it to simply calculate the fields or insert it into one of the most commonly used electromagnetic simulation tools: HFSS from Ansoft [17].

III. Obtaining the Cartographies

To obtain the tangential electric and magnetic field cartographies necessary to build the model, an automated near-field test bench is used.

A. Near-Field Test Bench

The near-field test bench developed within our research institute, the Embedded Electronic Systems Research Institute (IRSEEM) [14], is constituted by a five-axis robot with a mechanical resolution of 10 μm in the three directions (x, y, and z) and with 0.009° for the two rotations. The maximum scanning area is 200 cm (x) × 100 cm (y) × 60 cm (z).

A probe is set up on the robot arm which, commanded by a PC, moves it above the circuit; the data picked up by the probe are measured by a vector network analyzer (VNA) or a spectrum analyzer [18], and they are then saved on the PC. These data (voltage) are converted into electric and magnetic fields (in magnitude and phase) by means of a probe calibration using a wire above a ground plane (see [1], [19], and [20]).

B. Measurement Probes

Depending on the component of the field to be measured, different kinds of probes are used.

An electric dipole is used to pick up both tangential electric field components (E_x and E_y) rotating the probe 90° in the z-axis [19]. The dipole is made with two adjacent coaxial cables, and it is balanced using a 180° hybrid coupler whose working frequency range is from 30 to 3000 MHz and which helps us to suppress the common mode coupling. Each arm of the dipole is 3 mm in length, and they are made from the center conductor of the coaxial cables.

To measure the normal component of electric field (E_z), we use a 50-Ω open-end coaxial cable with a small ground plane in its extremity to improve its performance [20]. This probe must be placed perpendicularly to the DUT to measure the normal E-field.

The last probe [1] measures the magnetic field. It is based on a small loop, whose surface is 3.14 mm^2, made from the center conductor of two adjacent coaxial cables. The 180° hybrid coupler is also used as a balun. The loop measures the magnetic field perpendicular to its surface, so one probe allows us to get the tangential components (H_x and H_y) and another one, which is 90° curved, allows us to get the normal component (H_z).

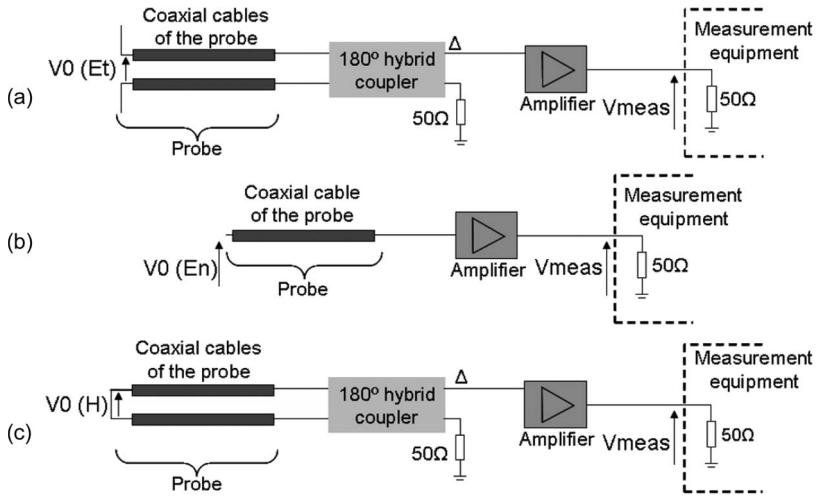

Fig. 2. Measurement chains for fields. (a) Tangential electric components x and y. (b) Normal electric component z. (c) All components of magnetic field.

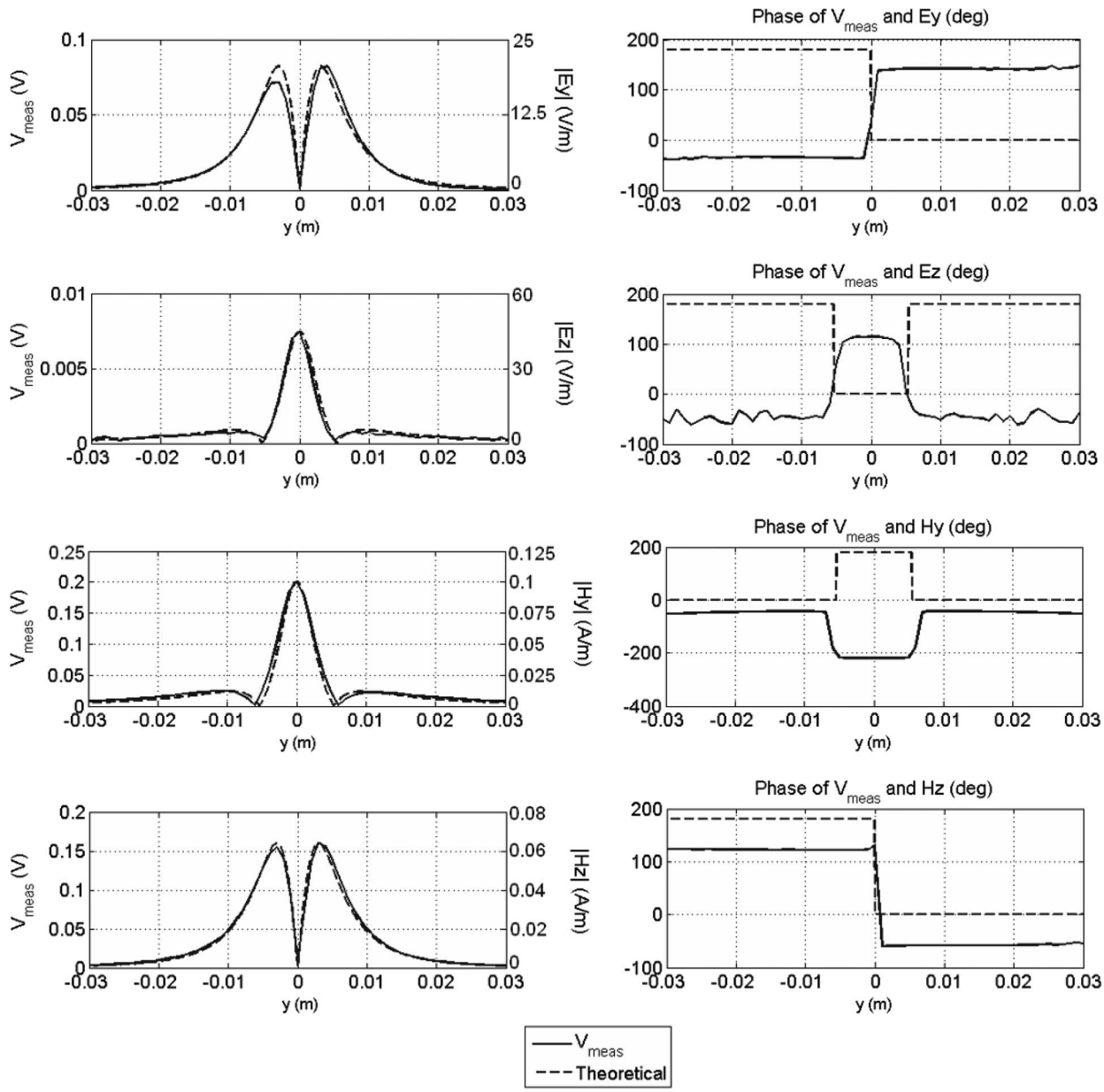

Fig. 3. Theoretical E and H fields and corresponding measured voltages at 2 mm above the wire above the ground plane.

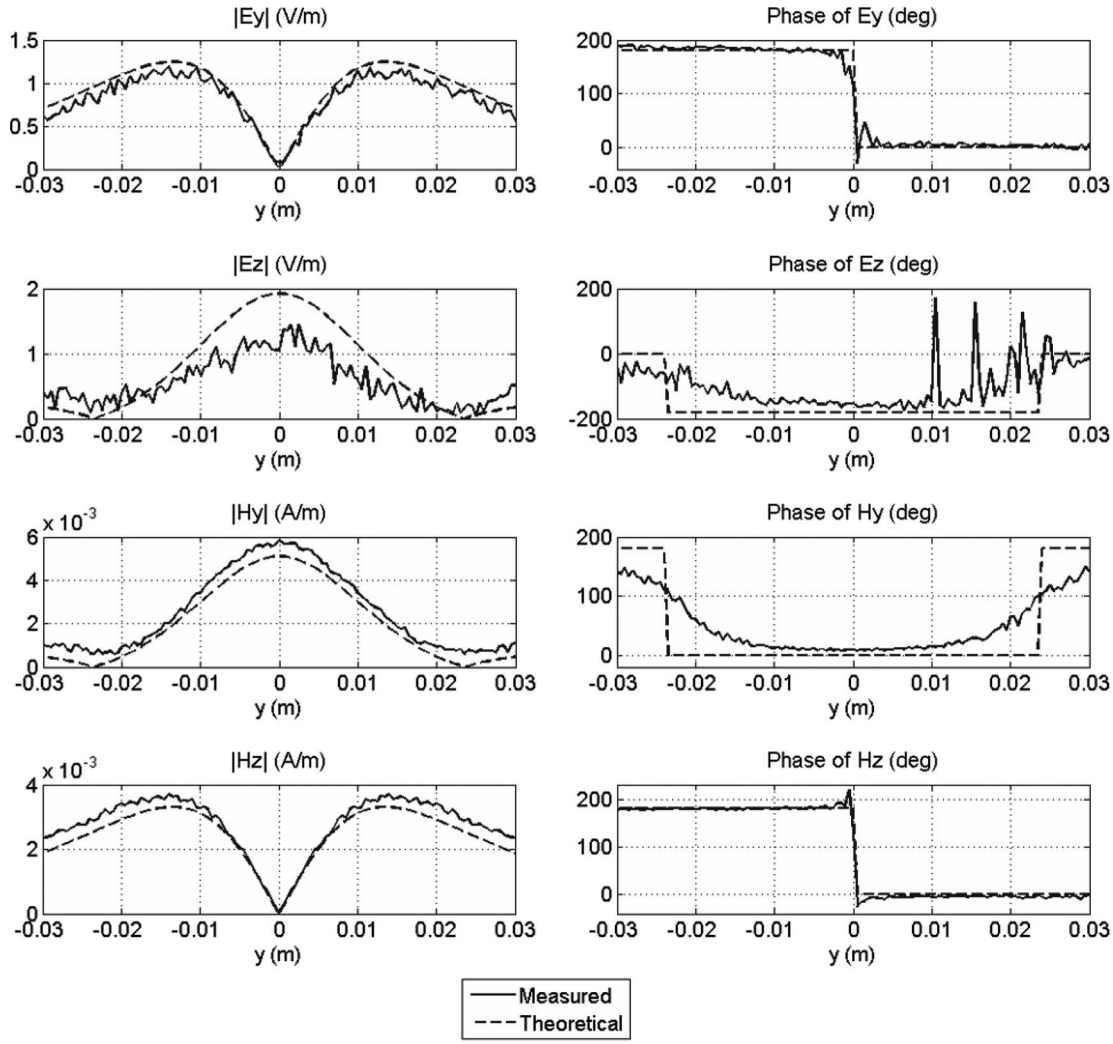

Fig. 4. Measured and theoretical E and H fields at 20 mm above the wire above the ground plane.

C. Measurement Chains and Calibration Process

The probes used are mismatched at the measurement frequency; their dimensions are very small in comparison with the wavelength to avoid too much disturbance of the natural radiation of the devices. Thus, to improve the sensitivity of the measurement, a low noise amplifier is added between the probes and analyzers.

Fig. 2 shows the measurement chains for the different probes.

The calibration consists, therefore, in obtaining the antenna factor a which links the voltage V_{meas} (output voltage of the amplifier) and the field measured by the probe ($[E,H]_{\text{meas}} = aV_{\text{meas}}$). The radiation of a simple circuit, whose theoretical radiation $[E,H]_{\text{theo}}$ is known, is measured ($V_{\text{meas}'}$), and it is used to obtain a ($a = [E,H]_{\text{theo}}/V_{\text{meas}'}$).

D. Validation of the Calibration Process Using a Wire Above a Ground Plane

To calibrate the measurement chain, a wire above a ground plane power supplied by a generator and loaded by 50 Ω is used. The wire has a radius of 1.5 mm, its center axis is at 2.05 mm above the ground plane, and it is oriented following the x-axis. The theoretical expressions of its radiated electric and magnetic fields are well known [1], and the y and z components are needed.

To obtain the antenna factors of the four probes defined in Section III-C as the ratio between the field and the measurement voltage V_{meas}, the fields are measured in a cross section at 2 mm above the wire. Fig. 3 shows a comparison between the measured voltage (V_{meas}) and the theoretical fields. We can appreciate that the probes keep the profile of the fields perfectly.

Using these data, the antenna factors are calculated at 967 MHz: $286e^{-j141^\circ}$ for the tangential electric components, $4945e^{-j114^\circ}$ for the normal electric component, $0.5e^{j39^\circ}$ for the tangential magnetic components, and $0.4e^{j59^\circ}$ for the normal magnetic component.

In order to validate the calibration, the same circuit is used. The antenna factors are applied to the voltages measured by the VNA corresponding to the fields radiated at 20 mm. Fig. 4 shows a comparison between the measured tangential and normal electric and magnetic fields (in amplitude and phase) and the theoretical values.

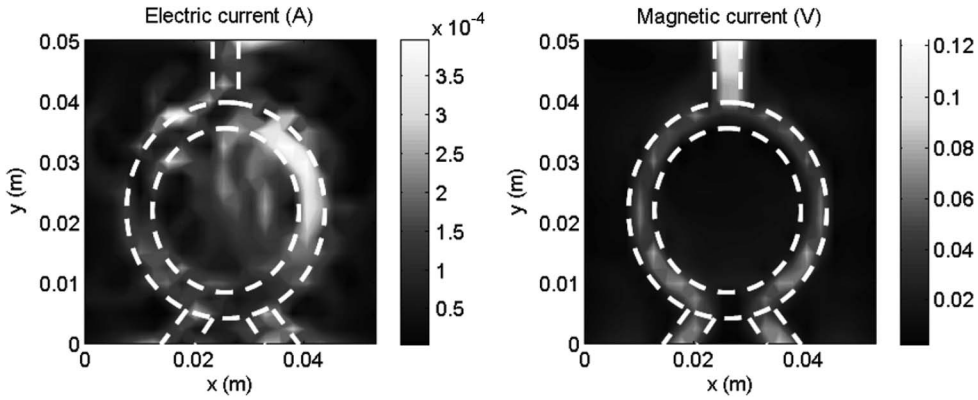

Fig. 5. Electric and magnetic currents through the dipoles.

In general, we obtain a good accordance in the amplitude and phase. Nevertheless, a difference in the level for E_z at 20 mm occurs. That can be due to a lack of sensitivity of the monopole at 20 mm and the presence of the square ground that can disturb the wire for low distances. Anyway, this component of the field is not used to build the model, so these differences will not disturb our modeling procedure.

IV. Application to a Wilkinson Power Divider

In practice, when measuring a "simple" device (e.g., passive circuits based on tracks), it is sometimes possible to validate certain aspects of the measurements (level, shape, etc.) with theoretical analysis or numerical simulation. In general cases (active, complex circuits, etc.), the electromagnetic behavior could not be foreseen, and the measurement will directly be the reference to build the model. Therefore, it is important to control the measurement process well.

In this section, we validate the process of the measurement and the calibration, comparing the measured cartographies to the HFSS simulations. To do that, a Wilkinson power divider built in microstrip technology (the relative permittivity of the substrate is $\varepsilon_r = 4.4$ and its thickness is $h = 1.6$ mm) and working at 967 MHz is used (its shape is represented in dotted lines in Fig. 5). Then, the procedure of the modeling is applied to this device, using the measurements to validate it, and finally, the insertion of the model into HFSS is also explained.

In [21], we have validated our modeling approach using the cartographies obtained from HFSS simulation. Indeed, working from numerical simulations allows avoiding the inaccuracy due to the orientation, position, and influence of the measurement probe. In this paper, we present the complete modeling process of the electromagnetic field from near-field measurements.

A. Validation of Measurements

Even if only the components x and y are needed to build the model, the z component has been also measured to validate it. The scanned surface has an area of 53 mm $(x) \times 50$ mm (y), and the number of measured points is 22 in the x-axis and 21 in the y-axis (462 points in total).

TABLE I
Errors Between Simulations and Measurements at 2 mm

E_x	E_y	E_z	H_x	H_y	H_z
0.4003	0.5646	0.1256	0.2304	0.8016	0.4822

In [21], a comparison between the measurements and HFSS simulations (in amplitude and phase) of the divider at 2 mm above it is shown.

To quantify the differences, we define the following error

$$\text{error} = \sum_{i=1}^{M} \left(\frac{|f_{\text{simu}}(M_i) - f_{\text{meas}}(M_i)|^2}{\sum_{j=1}^{M} |f_{\text{simu}}(M_j)|^2} \right) \tag{14}$$

where f can be an electric or magnetic field, M is the number of measurement points, and M_i is the point where the field is evaluated.

The evaluated errors for all the components of the fields at 2 mm are in Table I. We notice a few differences in the level, but the good correlation between the curves allows the validation of our measurements.

B. Study of the Parameters of the Model

The model is built from the near-field cartographies at 2 mm above the circuit. The set of dipoles consists of 462 electric dipoles and 462 magnetic dipoles. They are placed in the same positions in x and y as the measurement points but at a different height: the magnetic dipoles are in $z = 0$, and the electric dipoles are placed lower $(z = -0.6$ mm). This difference in location avoids the overlapping of the two sources when the model will be inserted into HFSS.

Fig. 5 shows the electric I_e and magnetic I_m currents obtained by the modeling. We can notice that the currents are on the metallic parts of the circuit. Therefore, it can be possible to identify the real sources of radiation for the simple components.

C. Validation of the Model

Using the set of dipoles obtained by modeling from the cartographies at 2 mm, we calculate the $\vec{E}$ and $\vec{H}$ fields at the same height to validate the process.

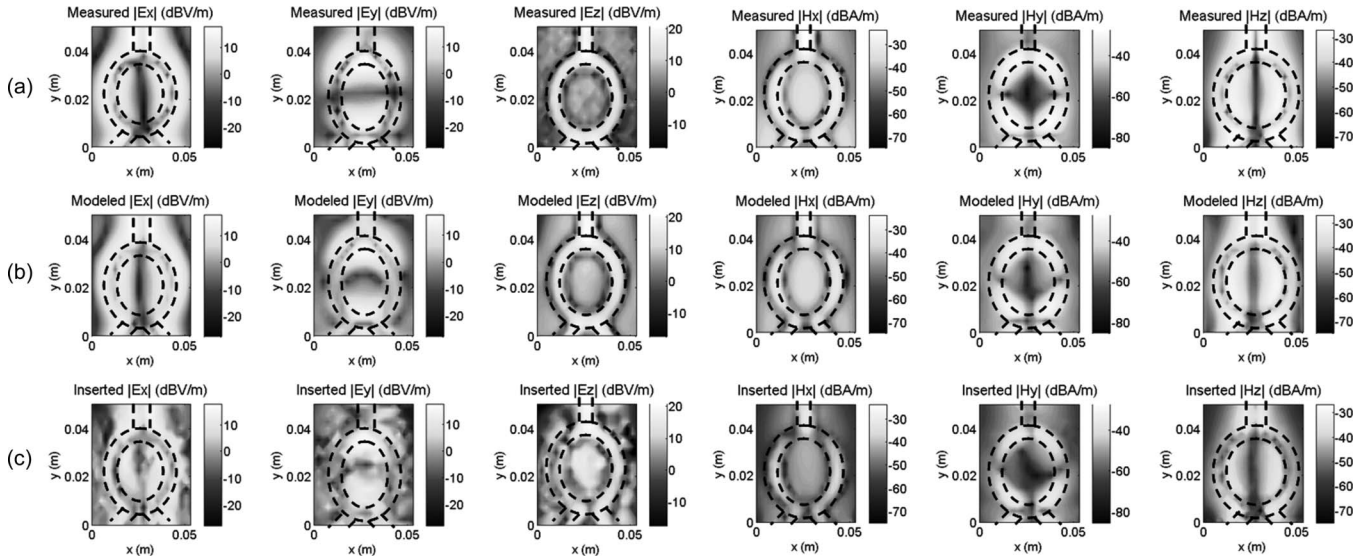

Fig. 6. Magnitude of E and H fields at 5 mm. (a) Measurements. (b) Modeling. (c) Insertion into HFSS.

TABLE II
ERRORS BETWEEN MEASUREMENTS AND MODELING

	E_x	E_y	E_z	H_x	H_y	H_z
2 mm	0.0629	0.1393	0.5779	0.0081	0.0112	0.1223
5 mm	0.0710	0.2175	0.3620	0.1200	0.1168	0.1205

Then, using this set of dipoles, the fields are evaluated at a higher distance: 5 mm. Fig. 6(a) and (b) shows a comparison between the measurements and the modeling for the $\vec{E}$ and $\vec{H}$ fields (in amplitude) at 5 mm above the divider.

The calculation of the model in MATLAB (from MathWorks) [12] takes 56 s in a CPU of 1-GB RAM and 1.86 GHz, and the simulation of the model to obtain the fields at one height takes 6 s.

Using (15), the errors for each component at 2 and 5 mm are evaluated. They are shown in Table II

$$\text{error} = \sum_{i=1}^{M} \left(\frac{|f_{\text{meas}}(M_i) - f_{\text{mod}}(M_i)|^2}{\sum_{j=1}^{M} |f_{\text{meas}}(M_j)|^2} \right). \qquad (15)$$

In spite of the slight differences, these results show that our model is able to reconstruct the field at the same height at which the cartographies were obtained (d) and can also determine the z component of the fields (component not used to build the model). A very good accordance between the modeling and the measurement at a distance above d, in magnitude and phase, is obtained. This allows us to completely validate the modeling process from the measurements, and it proves that it is possible to recreate the $\vec{E}$ and $\vec{H}$ near fields above the device.

D. Integration Into a Commercial Electromagnetic Simulator

The model has been developed to be suitable for a commercial simulation tool because several powerful electromagnetic simulation software, such as HFSS, are available in an industrial environment.

The insertion of a set of electric dipoles into HFSS has been already validated using a macro developed in Microsoft Visual Basic. The algorithm to insert a set of N equivalent dipoles is presented in [22] and [23]. The representation of an electric dipole into HFSS is a very thin rectangle in which a current source is applied to.

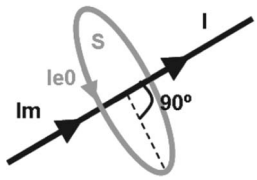

Fig. 7. Equivalence between a magnetic dipole and an electric loop.

To insert a magnetic dipole, we take into account its equivalence to an electric loop perpendicular to it (see Fig. 7). The relation between the electric loop and the magnetic dipole is given by the following expression

$$I_m l = j\omega\mu S I_{e0} \qquad (16)$$

where I_m is the magnetic current through the magnetic dipole, l is the length of the magnetic dipole, ω is the angular frequency, S is the surface of the loop, and I_{e0} is the electric current. The representation of an electric loop into HFSS is performed with current lines. Indeed, the electric loop is actually discretized into four segments (four electric dipoles) with a current value of I_{e0}. The process of insertion is, then, the same as that used for the electric dipoles with current I_e.

The fields shown in the previous section are radiated by a set of 462 electric dipoles and 462 magnetic dipoles uniformly spread. In order to reduce the number of sources, we have chosen those with a current value higher than a certain threshold. For the electric dipoles, the threshold is 30% of the maximum value of I_e, and for the magnetic dipoles, it is 20% of the maximum value of I_m. With this criterion, 158 electric dipoles and 94 magnetic dipoles are selected.

This reduction makes the insertion into an electromagnetic simulator easier because it decreases the insertion time and requires less computer memory. The set of dipoles inserted into

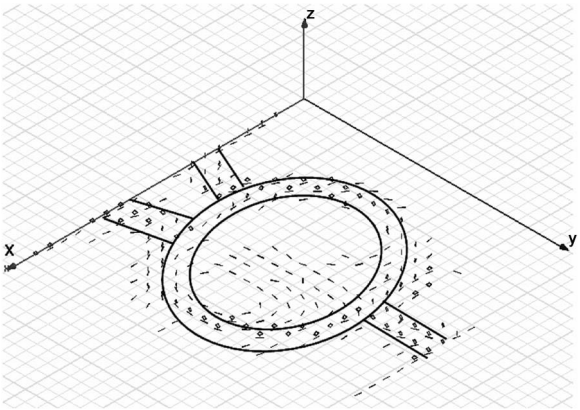

Fig. 8. Set of equivalent dipoles in HFSS.

TABLE III
ERRORS BETWEEN MEASUREMENTS AND INSERTION IN HFSS AT 5 mm

E_x	E_y	E_z	H_x	H_y	H_z
0.2836	0.5296	0.6694	0.4086	0.3849	0.3560

HFSS is shown in Fig. 8. The shape of the divider is also shown, but it is not in HFSS.

Fig. 6(a) and (c) shows the fields calculated in HFSS from the reduced set of dipoles compared to the measurements (in amplitude) at 5 mm.

The differences in the level are quantified in Table III. We find a good agreement between the inserted model and the measurements at a distance different from the height at which the cartographies were obtained (2 mm).

Therefore, we have also validated the insertion of the model into a commercial electromagnetic simulation tool.

The simulation time of the model to obtain the fields in HFSS (version 10) is 1 h, whereas in MATLAB, it is 3 s (for a single height) using a CPU of 2-GB RAM and 2.26 GHz. Thus, if the user only wants to calculate the fields at different heights, the simulation of the model in MATLAB is more interesting than that in HFSS. However, HFSS can enable the user to study the coupling between a disturbing source and a victim.

Nevertheless, our model has some limitations. As we use near-field measurements, its accuracy depends on the validity of the measurements of the fields. The rise in frequency, the sensitivity, and the resolution of the probe can also be sources of errors.

V. DISCUSSION ABOUT THE MODELING PROCEDURE

A. Modeling an Active Circuit

The methodology of the modeling has also been applied to an active circuit: an oscillator which consists of a quartz and some inverters working at 40 MHz [24]. The board is power supplied by a 9-V battery placed under the ground plane, so no wires are required to power supply it. The model is built from the measurements at 2 mm and is composed of 961 electric dipoles and 961 magnetic dipoles.

Fig. 9 presents the variation of the electric and magnetic fields as a function of the distance above the oscillator of up to 11 cm (maximum distance at which the magnitude of the measured field is above the noise level using the near-field test bench). An acceptable agreement occurs between the modeling and the measurements, particularly for the magnetic field. The differences for the electric field are due to the lack of sensitivity of the E_z probe at high distances.

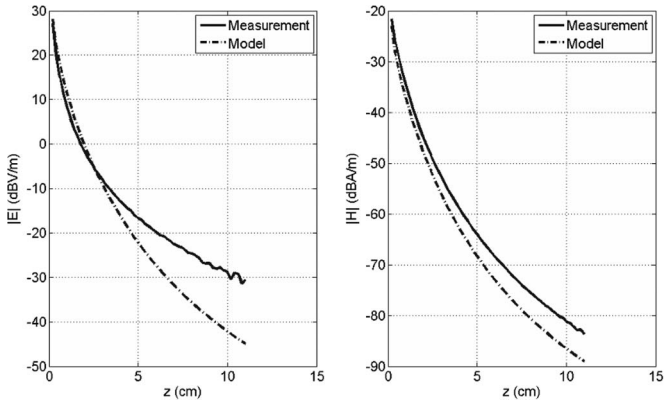

Fig. 9. Electric and magnetic field variation as a function of the distance above the device.

TABLE IV
VALUES FOR ELECTRIC FIELD AT 3 m

	E_x (dBμV/m)	E_y (dBμV/m)
Measurement	15.01	13.03
Modeling	9.39	7

To complete the study, a horizontal and vertical polarized electric-field measurement at 3 m from the oscillator has been made in an anechoic chamber. The model has also been used to evaluate the x and y components of the electric field at the same distance. From Table IV, we notice a difference of 6 dB for each component between the measurement and the modeling. In spite of this gap, our model can give a quite good estimation of the electric-field level in the far field.

The insertion of the model into HFSS has been also validated in [24] with a reduction of the number of dipoles (133 electric dipoles and 64 magnetic dipoles).

B. Influence of the Thresholds of Current

In Section IV-D, the set of dipoles has been reduced to make possible the insertion into HFSS. To do so, we have defined two threshold limits on the electric and magnetic currents in order to keep the dipoles whose current magnitudes are greater than these thresholds.

This section presents the influence of these limits on the Wilkinson power divider in two steps. The first one consists in varying the threshold of the magnetic current keeping the threshold of the electric current constant (30%), and in the second step, we do the inverse (with a magnetic current threshold of 20%). The errors [calculated using (15)] for the electric and magnetic fields are presented in Fig. 10.

Obviously, the lower the threshold is, the smaller the error is. Therefore, to reduce the model, the user must make a tradeoff between the number of dipoles and the accuracy in the prediction of the fields.

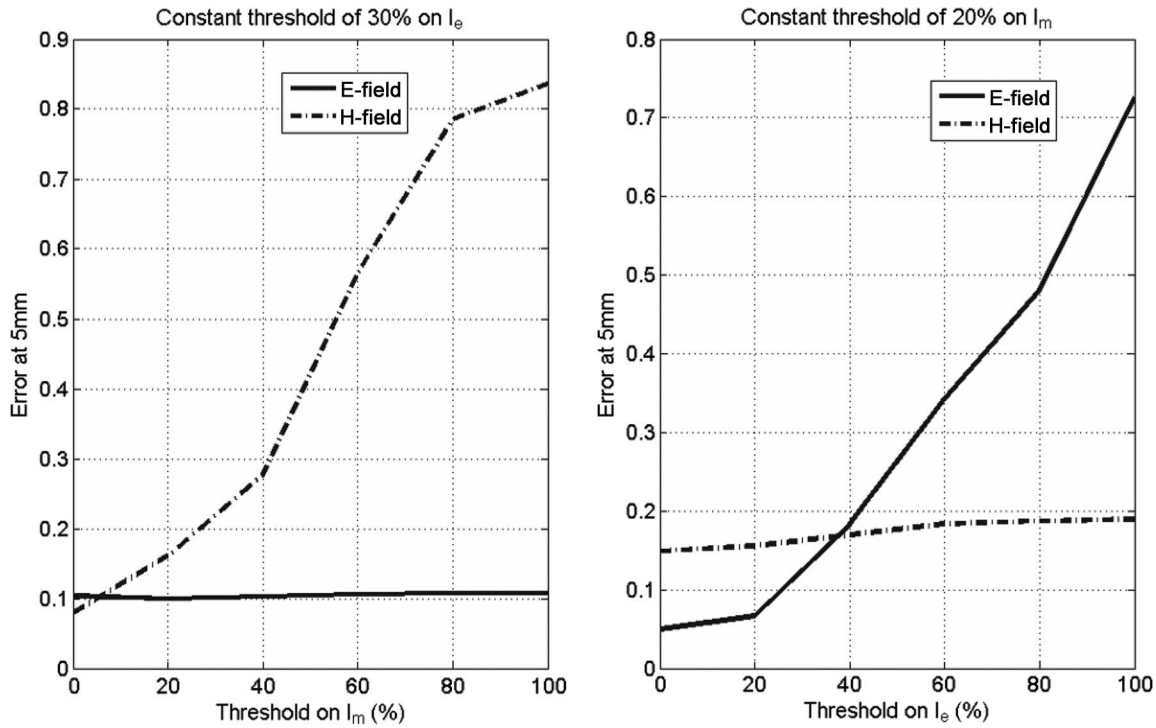

Fig. 10. Error between the E- and H-field measurements and modeling (reduced set of dipoles) for different thresholds.

TABLE V
ERRORS BETWEEN MEASUREMENTS AND DISTURBED MEASUREMENTS AND MODELING

	E_x	E_y	E_z	H_x	H_y	H_z
Meas (2mm)	0.0590	0.0863	-	0.0374	0.0756	-
Mod (2mm)	0.0917	0.1859	0.6368	0.0479	0.0855	0.1253
Mod (5mm)	0.0705	0.2212	0.4005	0.1160	0.1032	0.1121

C. Study of the Conditioning

As explained previously (see Section II-B), an inverse problem can be ill-conditioned, so the disturbances on the measurements can hugely affect the solution. To study the influence of these possible disturbances in the case of the Wilkinson power divider, we consider a cross-field problem in the measurements. Thus, the disturbed measurements are expressed as

$$E'_x = \alpha E_x + \beta E_y + \gamma E_z \tag{17}$$

$$E'_y = \beta E_x + \alpha E_y + \gamma E_z \tag{18}$$

$$H'_x = \alpha H_x + \beta H_y + \gamma H_z \tag{19}$$

$$H'_y = \beta H_x + \alpha H_y + \gamma H_z \tag{20}$$

where α is a matrix of random values between -2 and $+2$ dB, β and γ are two random matrices whose values are between -0.2 and 0.2, and E_x, E_y, E_z, H_x, H_y, and H_z are the undisturbed measurements of the fields.

The model is built from these disturbed data at 2 mm, and then, the electric and magnetic fields are calculated at 5 mm above the device.

Row 1 of Table V shows the errors between the disturbed and undisturbed measurements at 2 mm, whereas rows 2 and 3 show the errors between the disturbed model and the undisturbed measurements at 2 and 5 mm using (15). Comparing these values to those in Table II, the errors are slightly debased.

A more in-depth and general study would be needed to go into detail about the numerical conditioning of the problem, but in the particular case of our Wilkinson power divider, the modeling procedure is not really dependent on the measurement disturbances. This subject still remains an open issue.

VI. CONCLUSION

This paper has proposed a simple methodology to model the near-field emissions of an electronic device based on a set of equivalent sources, and it has shown how to use the model with commercial electromagnetic simulation software. The results obtained on a Wilkinson power divider allow us to validate the modeling process and the electromagnetic measurements with our near-field test bench. Moreover, they show that it is possible to reconstruct the electromagnetic field above the component to model in the near-field region.

Once the model of the device is built, engineers can use it to simply evaluate the near fields; the results are obtained rather quickly (a few seconds) with MATLAB, for example. The modeling of an active circuit, such as an oscillator, allows validating the evolution of the fields as a function of the distance above it and allows estimating the electric far-field values at 3 m. This device is quite special because no interconnection

wires (i.e., no auxiliary devices) are required and the model comprises the whole oscillator (including the power supply).

The model can be inserted into HFSS as current lines. This step needs to reduce the number of dipoles to avoid a too long computational time and problems of memory. To make the model suitable for the HFSS, two thresholds must be defined, fixing a tradeoff between the number of dipoles and the accuracy of the model to limit the simulation time in HFSS.

Several studies are planned in prospect: the coupling of a circuit with printed-circuit-board tracks using theoretical analysis and electromagnetic simulations and the reduction of the number of sources using another methodology (inverse method and an optimization algorithm). A more in-depth analysis of the matrix conditioning is also planned.

To overcome the limitations of our model, we are currently working on an optic test bench to improve the resolution and to be able to work at high frequencies [25].

ACKNOWLEDGMENT

This paper is closely related to the program entitled "EMC Platform for Embedded Applications" of the Aerospace Valley Network, Midi-Pyrénées and Aquitaine world competitiveness cluster, France. Portions of this paper are reprinted or reused, by permission, from the Proceedings of the Fourth International Conference on Electromagnetic Near-Field Characterization and Imaging (ICONIC 2009), Copyright 2009, Oriental Institute of Technology. The authors would like to thank the reviewers for all their comments to improve this paper.

REFERENCES

[1] D. Baudry, C. Arcambal, A. Louis, B. Mazari, and P. Eudeline, "Applications of the near-field techniques in EMC investigations," *IEEE Trans. Electromagn. Compat.*, vol. 49, no. 3, pp. 485–493, Aug. 2007.

[2] H. Weng, D. G. Beetner, R. E. DuBroff, and J. Shi, "Estimation of current from near-field measurement," in *Proc. IEEE Int. Symp. Electromagn. Compat.*, Chicago, IL, Aug. 2005, vol. 1, pp. 222–227.

[3] F. de Daran, J. Chollet-Ricard, F. Lafon, and O. Maurice, "Prediction of the field radiated at one meter from microprocessors from near EM field cartography," in *Proc. IEEE Int. Symp. Electromagn. Compat.*, Istanbul, Turkey, May 2003, pp. 479–482.

[4] A. Taaghol and T. K. Sarkar, "Near-field to near/far-field transformation for arbitrary near-field geometry, utilizing an equivalent magnetic current," *IEEE Trans. Electromagn. Compat.*, vol. 38, no. 3, pp. 536–542, Aug. 1996.

[5] H. Fan and F. Schlagenhaufer, "Near-field—Far field conversion based on genetic algorithm for predicting radiation from PCBs," in *Proc. IEEE Int. Symp. Electromagn. Compat.*, Honolulu, HI, Jul. 2007, pp. 1–6.

[6] O. Aouine, C. Labarre, and F. Costa, "Measurement and modeling of the magnetic near field radiated by a buck chopper," *IEEE Trans. Electromagn. Compat.*, vol. 50, no. 2, pp. 445–449, May 2008.

[7] J. R. Regué, M. Ribó, J. Gomila, A. Pérez, and A. Martín, "Modeling of radiating equipment by distributed dipoles using metaheuristics methods," in *Proc. IEEE Int. Symp. Electromagn. Compat.*, Chicago, IL, Aug. 2005, pp. 8–12.

[8] Y. Vives-Gilabert, C. Arcambal, A. Louis, P. Eudeline, and B. Mazari, "Modeling magnetic emissions combining image processing and an optimization algorithm," *IEEE Trans. Electromagn. Compat.*, vol. 51, no. 4, pp. 909–918, Nov. 2009.

[9] C. Labussiere-Dorgan, S. Bendhia, E. Sicard, J. Tao, H. J. Quaresma, C. Lochot, and B. Virgnon, "Modeling the electromagnetic emission of a microcontroller using a single model," *IEEE Trans. Electromagn. Compat.*, vol. 50, no. 1, pp. 22–34, Feb. 2008.

[10] Y. Alvarez López, F. Las Heras Andrés, M. Rodríguez Pino, and T. K. Sarkar, "An improved super-resolution source reconstruction method," *IEEE Trans. Instrum. Meas.*, vol. 58, no. 11, pp. 3855–3866, Nov. 2009.

[11] J. Shi, M. A. Cracraft, J. Zhang, R. E. DuBroff, K. Slattery, and M. Yamaguchi, "Using near-field scanning to predict radiated fields," in *Proc. IEEE Int. Symp. Electromagn. Compat.*, Santa Clara, CA, Aug. 2004, vol. 1, pp. 14–18.

[12] MATLAB From MathWorks. [Online]. Available: http://www.mathworks.com

[13] C. Leseigneur, O. Kröning, P. Fernández López, D. Baudry, A. Louis, and M. Leone, "Analysis of transmission line coupling with a near-field excitation," presented at the 7th Int. Workshop Electromagnetic Compatibility Integrated Circuits, Toulouse, France, Nov. 2009, Paper 62.

[14] Y. Vives-Gilabert, C. Arcambal, A. Louis, F. de Daran, P. Eudeline, and B. Mazari, "Modeling magnetic radiations of electronic circuits using near-field scanning method," *IEEE Trans. Electromagn. Compat.*, vol. 49, no. 2, pp. 391–400, May 2007.

[15] C. A. Balanis, *Antenna Theory, Analysis and Design*, 2nd ed. New York: Wiley, 1997.

[16] H. Fan and F. Schlagenhaufer, "Investigation of near field data sampling approaches for far field radiation prediction of PCBs by genetic algorithm," in *Proc. 18th Int. Zurich Symp. Electromagn. Compat.*, Munich, Germany, Sep. 2007, pp. 21–24.

[17] HFSS (High Frequency Structure Simulator) From Ansoft. [Online]. Available: http://www.ansoft.com

[18] Y. Vives, C. Arcambal, A. Louis, B. Mazari, and P. Eudeline, "Measuring amplitude and phase of radiated electromagnetic near fields," in *Proc. 3rd ICONIC*, St. Louis, MO, Jun. 2007, pp. 27–32.

[19] L. Bouchelouk, Z. Riah, D. Baudry, M. Kadi, A. Louis, and B. Mazari, "Characterization of electromagnetic fields close to microwave devices using electric dipole probes," *Int. J. RF Microw. Comput.-Aided Eng.*, vol. 18, no. 2, pp. 146–156, Mar. 2008.

[20] D. Baudry, A. Louis, and B. Mazari, "Characterization of the open-ended coaxial probe used for near-field measurements in EMC applications," *Prog. Electromagn. Res.*, vol. PIER 60, pp. 311–333, 2006.

[21] P. Fernández López, C. Arcambal, S. Verdeyme, D. Baudry, and B. Mazari, "Near-field measurements to create a model suitable for a commercial simulation tool," in *Proc. 4th ICONIC*, Taipei, Taiwan, Jun. 2009, pp. 208–213.

[22] P. Fernández López, A. Ramanujan, Y. Vives Gilabert, C. Arcambal, A. Louis, and B. Mazari, "A radiated emission model compatible to a commercial electromagnetic simulation tool," in *Proc. 20th Int. Zurich Symp. Electromagn. Compat.*, Zurich, Switzerland, Jan. 2009, pp. 369–372.

[23] P. Fernández López, C. Arcambal, Y. Vives Gilabert, A. Ramanujan, D. Baudry, A. Louis, and B. Mazari, "Development of a magnetic near-field model and insertion into a commercial electromagnetic simulator," *Turkish J. Elect. Eng. Comput. Sci.*, vol. 17, no. 3, pp. 289–300, Nov. 2009.

[24] P. Fernández López, C. Arcambal, D. Baudry, S. Verdeyme, and B. Mazari, "Radiation modeling and electromagnetic simulation of an active circuit," presented at the 7th Int. Workshop Electromagnetic Compatibility Integrated Circuits, Toulouse, France, Nov. 2009, Paper 58.

[25] D. Chevallier, D. Baudry, A. Louis, and B. Mazari, "Study of near-field techniques for microelectronic applications," in *Proc. 4th ICONIC*, Taipei, Taiwan, Jun. 2009, pp. 199–202.

Priscila Fernández López was born in Oviedo, Spain, in 1982. She received the degree in telecommunication engineering from the University of Oviedo, Gijón, Spain, in 2007. She is currently working toward the Ph.D. degree in electronics at the University of Rouen, Mont Saint Aignan, France, and in the Embedded Electronic Systems Research Institute (IRSEEM), Saint Etienne du Rouvray, France.

Since 2006, she has been with IRSEEM. Her current research interests include electromagnetic compatibility, particularly the measurement and modeling of radiated emissions of electronic components.

Christian Arcambal was born in Chambéry, France, in 1976. He received the diploma in engineering from the Graduate Engineering School Ecole Supérieure d'Ingénieurs (ESIGELEC), Saint Etienne du Rouvray, France, in 1999, and the Ph.D. degree in electronics from the University or Rouen, Mont Saint Aignan, in 2003. His thesis took place in Thales Air Defence, Ymare, France, in collaboration with the Embedded Electronic Systems Research Institute (IRSEEM, the ESIGELEC Research Institute), Saint Etienne du Rouvray, France.

From 2004 to 2008, he was a Lecturer and Researcher with IRSEEM. His research activities were focused on electromagnetic compatibility (EMC) for automotive applications and component EMC in terms of measurement and modeling. He is currently with the Commisariat à l'énergie atomique et aux energies alternatives, Centre de Saclay, Gif-sur-Yvette, France, where he is working on the EMC aspects for space applications.

David Baudry was born in Paris, France, on August 14, 1974. He received the diploma in engineering (equivalent to M.Sc.) for the Ecole Nationale Supérieure d'Ingénieurs, Caen, France, in 1999, and the Ph.D. degree in electronics from the University of Rouen, Mont Saint Aignan, France, in 2005.

From 2000 to 2001, he was with the Sopra Group and was involved in software development. In 2001, he was with the Graduate Engineering School Ecole Supérieure d'Ingénieurs (ESIGELEC), Saint Etienne du Rouvray. He is currently with the Embedded Electronic Systems Research Institute (IRSEEM, the ESIGELEC Research Institute), Saint Etienne du Rouvray, France, where he is a Lecturer and the Deputy Head of the Electromagnetic Compatibility (EMC) Team. His research interests include near-field measurements for EMC applications, electromagnetic simulations, and modeling.

Serge Verdeyme (M'99) was born in Meilhards, France, in June 1963. He received the doctorat degree from the University of Limoges, Limoges, France, in 1989.

He is currently a Professor with the XLIM Laboratory, University of Limoges, where he is the Head of the Micro et Nanotechnologies pour Composants Optoélectroniques et Microondes Department. His main research interests include the design and optimization of microwave devices.

Bélahcène Mazari (M'06) was born in Oujda, Morocco, on March 15, 1958. He received the Ph.D. degree in electromagnetism from the University of Rouen, Mont Saint Aignan, France, in 1988, and was entitled for supervising research in 2004.

Since 1987, he has been a Professor of electromagnetism and electronics with the Graduate Engineering School Ecole Supérieure d'Ingénieurs (ESIGELEC), Saint Etienne du Rouvray. In 2001, he was one of the driving forces in the creation of the Embedded Electronic Systems Research Institute (IRSEEM, the ESIGELEC Research Institute), and has been working since then as a Manager for the institute. In 2008, he has taken on the position of Deputy Managing Director in charge of the development and research of ESIGELEC. He is a key player in the automotive, aerospace, and more widely speaking electronics' domains of the Haute-Normandie Region.